Synthesis of $YBa_2Cu_3O_{7-\delta}$ and Y_2BaCuO_5 Nanocrystalline Powders for YBCO Superconductors Using Carbon Nanotube Templates

Yunhua Shi,[†] Tawfique Hasan,[†] Nadendla H. Babu,[‡] Felice Torrisi,[†] Silvia Milana,[†] Andrea C. Ferrari,[†,*] and David A. Cardwell[†]

[†]Department of Engineering, University of Cambridge, Cambridge, CB2 1PZ, U.K., and [‡]BCAST, Brunel University, Uxbridge, UB8 3PH, U.K.

ABSTRACT

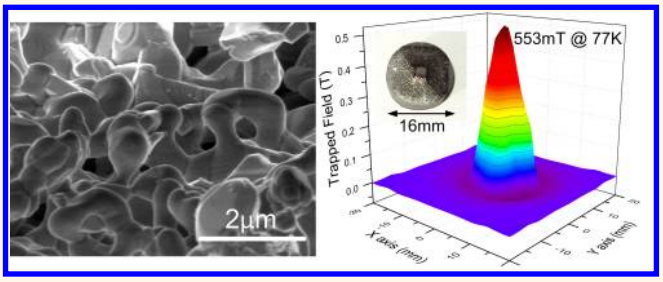

We fabricate nanosized superconducting $YBa_2Cu_3O_{7-\delta}$ (Y-123) and nonsuperconducting Y_2BaCuO_5 (Y-211) powders using carbon nanotubes as template. The mean particle size of Y-123 and Y-211 is 12 and 30 nm, respectively. The superconducting transition temperature of the Y-123 nanopowder is 90.9 K, similar to that of commercial, micrometer-scale powders fabricated by conventional processing. The elimination of carbon and the formation of a high purity superconducting phase both on the micro- and macroscale is confirmed by Raman spectroscopy and X-ray diffraction. We also demonstrate improvement in the superconducting properties of YBCO single grain bulk samples fabricated using the nanosize Y-211 powder, both in terms of trapped field and critical current density. The former reaches 553 mT at 77 K, with a ~20% improvement compared to samples fabricated from commercial powders. Thus, our processing method is an effective source of pinning centers in single grain superconductors.

KEYWORDS: superconductivity · flux pinning · nanotubes · trapped field

The superconducting properties of high-temperature superconductors (HTS), such as Y–Ba–Cu–O (YBCO), depend strongly on their microstructure.[1] In particular, the critical current density, J_c, a key parameter for applications,[2] is proportional to the number of pinning centers per unit volume in the superconducting phase.[3] Nonsuperconducting phases with small dimensions (in the nanometer range) within the superconducting matrix form particularly effective flux pinning centers in YBCO. These can generally be described as defects and nonsuperconducting second phases, which "pin" the quantized magnetic flux lines within the interior of a current carrying type II superconductor.[4] In particular, defects caused by neutron irradiation significantly increase J_c.[5] The introduction of nanostructured secondary phases, such as Y_2BaCuO_5 (Y-211), ZrO_2,[6] and $Y_2Ba_4CuMO_y$ (Y-2411(M)) (where M = Nb, W, Zr, Ag, Bi, *etc.*) into the Y-123 superconducting phase has also long been the focus of bulk HTS research.[7−9] However, these secondary phases tend to form either inclusions, up to several micrometers in size, or agglomerates[10] during the high temperature process used to prepare the bulk material.[7,11−13] Thus, it is desirable to develop new methods to reduce the second-phase particle size, in order to improve flux pinning, hence J_c.

Bulk YBCO superconductors are commonly processed using the so-called top seeded melt-growth (TSMG) technique.[11,12] This involves mixing the Y-123 and Y-211 precursor powders in the required stoichiometric ratio, and then pressing them uniaxially to form pellets of the desired shape. A seed crystal is placed on top of this pellet, and the whole assembly is melt-processed to form a single grain.[11,12] The seed crystal promotes epitaxial heterogeneous nucleation and facilitates the growth from the melt.[11,12,14] In bulk YBCO, the resultant microstructure consists typically of Y-211 particles embedded in a single-crystal Y-123 matrix.[2,11,12] These Y-211 particles enhance magnetic flux pinning, which improves the current carrying capacity of the superconductor.[11,15] One of the key challenges for enhancing the magnetic flux pinning is to reduce the size of the Y-211 particles in the Y-123 matrix.[15] In the case of bulk HTS

* Address correspondence to acf26@eng.cam.ac.uk.

Received for review March 22, 2012 and accepted May 28, 2012.

Published online May 28, 2012
10.1021/nn301262t

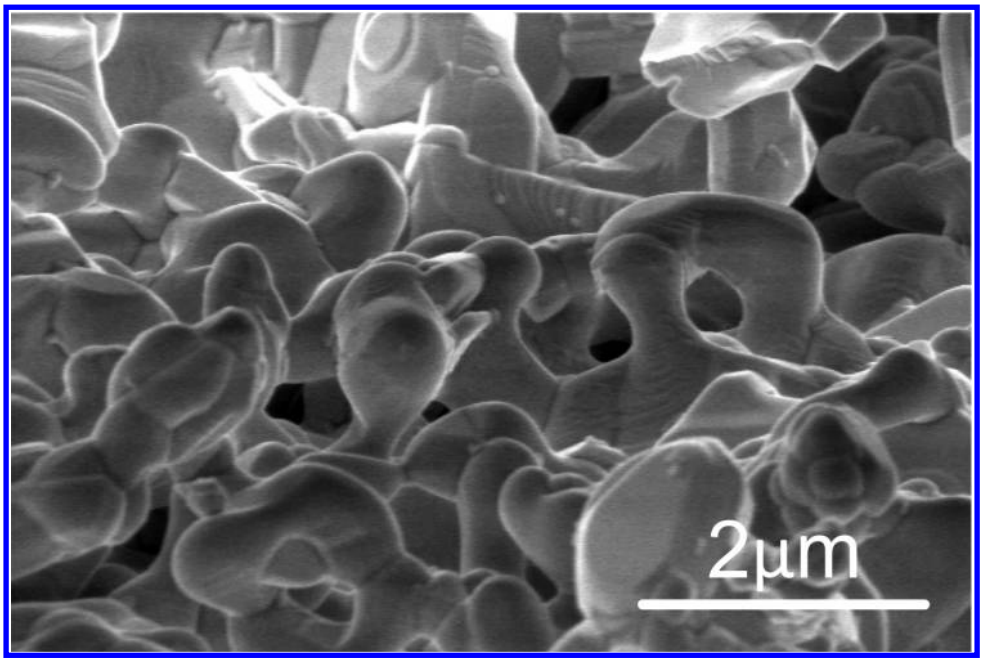

Figure 1. SEM photograph of powder A1 calcined at 880 °C.

superconductors, the size of the particles that are mixed together and pressed to form the pellets is crucial in achieving high J_c. However, the mean particle size of commercially available powders is typically $\sim 1-3\ \mu$m.[16] This is a consequence of their production by conventional solid-state reactions at elevated temperatures.[11,12] To fabricate a more homogeneous, finer powder, research has been carried out on improving the powder melting process, and combining this with ball milling,[17] or wet chemical synthesis of RE-123 or RE-211 precursors (where RE = Nd, Sm, Y),[9,18−20] *e.g.,* spray-drying[19] and coprecipitation[9] yield microstructured ($1-2\ \mu$m) Nd-123 and Y-123 powders with a homogeneous particle size distribution. Even better results may be achieved if the reaction is carried out in a controlled environment.[18,20−22] For example, ref 20 used solution-based nanoemulsions to produce Y-211 powders with a particle size distribution between 30 and 100 nm (although the superconducting properties of the bulk sample fabricated using this Y-211 were relatively poor). Extensive ball milling is also an effective way of reducing particle size.[23] However, the particle size typically produced by this technique is limited to several hundred nanometers, which is relatively large compared to the coherence length, therefore does not yield optimum flux pinning. Extensive ball milling also introduces impurities into the precursor powder, which complicates the processing and can limit the superconducting properties of bulk (RE)BCO samples fabricated by TSMG.

Carbon nanotubes (CNTs) can be used as template for the fabrication of wires and tubes of various metals and metal-oxides,[24] by filling or coating them with the desired material.[24−27] The aim of most previous work was to retain the shape/structure of the CNT templates.[24,27] Here we employ CNTs as template for nanosized Y-211 and Y-123 powders, then used to fabricate bulk superconductors, but without the need to retain the CNT shape. We obtain Y-123 and Y-211 flake-like structures, rather than a solid, regular coating. These are then ground and calcined to produce nanosized powders. Y-211 is chosen because it forms effective second phase flux pinning centers in YBCO.[15] We also fabricate Y-123 powders using the same methodology to confirm that carbon is eliminated during the process. This is important because the superconducting transition temperature (T_c) of Y-123 is particularly sensitive to the presence of impurities.[28] Elimination of carbon and the formation of a high purity of a superconducting phase on both micro- and macroscales is confirmed by Raman spectroscopy and X-ray diffraction (XRD). We then fabricate YBCO nanostructured powders (Y-211−30 nm and Y-123−12 nm, with $T_c \approx 90.9$ K) and a bulk sample using the nanostructured Y-211, with a ~20% improvement in J_c compared to a bulk sample prepared using commercial micrometer-sized powders.

The use of nanotemplating to fabricate nanosize phases of secondary inclusions reported here avoids contamination of the precursor powder with impurities, which is an inevitable consequence in powders produced by extensive ball milling, or by other methods, in the TSGM process. The nanosize powders reported here are not only impurity-free, but are also an order of magnitude smaller than precursor powders fabricated by extensive ball milling, with a much closer match to the superconducting coherence length, therefore to the optimum flux pinning. Thus, our novel approach is a

viable alternative to conventional powder processing, and the nano Y-211 secondary phase formed using nanotemplating is an effective source of pinning centers in single grain bulk superconductors.

RESULTS AND DISCUSSION

We use multiwall CNTs (MWNTs) as they can be dispersed by low power sonication in water or other solvents, similar to single wall carbon nanotubes,[29,30] but offer a significantly cheaper alternative. MWNT powder (Sigma-Aldrich[31]) is sonicated and centrifuged as discussed in the Methods section. After the removal of unexfoliated bundles by centrifugation, the MWNT dispersion is mixed ultrasonically with a Y-123 nitrate aqueous solution. The resulting liquid mixture is then dried (sample A). The corresponding Y-211-MWNT mixture is prepared following the same approach (sample B). The fully dried samples are calcined to eliminate nitrates and produce nanostructured powders, samples A1 and B1. These are ground further and calcined repeatedly until XRD confirms the formation of the Y-123 (sample A2) and Y-211 (sample B2) phases. Note that repeated grinding and high temperature calcination, necessary steps for the fabrication of Y-123 and Y-211, increase the particle size significantly.[4,7,11,12] The T_c of sample A2 and commercially available Y-123 powder (99.9% purity)[16] are then compared to assess the superconducting properties of sample A2, since the presence of even a small amount of carbon in the Y-123 lattice is known to reduce T_c significantly.[32] For example, 0.5 wt % carbon would cause T_c to decrease by several degrees.[32] Raman spectroscopy of the precursors (A,B) and ground samples (A2, B2) is used to monitor the presence of MWNTs or carbonaceous impurities. Raman spectroscopy also probes the formation of Y-123 and Y-211 phases in A2 and B2.

YBCO single grains are fabricated from sample B2 and commercially available Y-123 powder *via* TSMG.[11,12] To assess the superconducting properties of the samples derived with our new process, a single grain YBCO is also grown by TSMG using commercial Y-123 and Y-211 powders (see Methods for fabrication and characterization details).

Figure 1 shows a scanning electron microscope (SEM) image of sample A1 after secondary calcination in air at 880 °C, but prior to grinding. No MWNTs can be seen, since they decompose into CO and CO_2 during calcination. The layered flake-like microstructure may be due to the formation of anisotropic tetragonal or orthorhombic Y-123 phases on the MWNT outer surface.

Unpolarized Raman spectra are acquired at 632.8 nm excitation using a Renishaw InVia spectrometer, with a 100× objective. We use this wavelength to enhance detection of the carbon species.[33] Figure 2a compares the Raman spectra of the MWNT powder with the

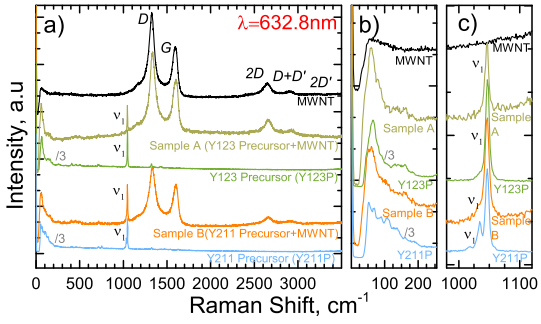

Figure 2. (a) Raman spectra of MWNTs, nitrate-MWNT dried precursor samples (A, B), and precursor nitrate salt mixtures (Y123P, Y211P). (b) Low frequency region; (c) symmetric in-phase N−O stretching from the precursor nitrates.

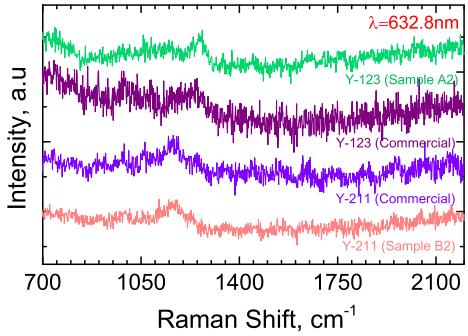

Figure 3. Raman spectra of samples A2 and B2 and their commercial Y-123 and Y-211 counterparts at 632.8 nm excitation.

precursor salts/MWNT mixtures. The MWNT sample shows prominent D, G, 2D, D+D′ and 2D′ peaks, Figure 2a. The G peak is present in any sp^2 carbon material and is due to the relative motion of carbon atoms, regardless of whether they are arranged in rings or chains.[34] Confinement and curvature split this band into G^+ and G^- peaks in single-wall CNTs.[35] However such splitting is not observed due to the large diameter of our nanotubes (inner diameter 5−10 nm, outer diameter 10−20 nm).[31] The D peak is a "breathing mode" of sp^2 bonded carbon atoms in 6-fold rings and requires the presence of defects for its activation.[34] The relative intensity of the D to G peaks, $I(D)/I(G)$, can be used to quantify the amount of disorder.[34,36,37] Our measured $I(D)/I(G)$ is consistent with that usually reported for the chemical vapor deposited (CVD) MWNTs used here.[38,39]

In the low frequency region, the radial breathing modes (RBMs) are observed. Their position Pos(RBM), is inversely related to nanotube diameter (d) by $\mathrm{Pos(RBM)} = (C_1/d) + C_2$.[40] A variety of C_1 and C_2 were proposed for this relation.[40−44] Here we use $C_1 = 214.4\ \mathrm{cm^{-1}}$ nm and $C_2 = 18.7\ \mathrm{cm^{-1}}$, from ref 40. These were derived by plotting the resonance energy as a function of inverse RBM frequency without any additional assumptions. Given the $\sim 35\ \mathrm{cm^{-1}}$ cut off frequency of our notch filter, according to the above relation, we are able to observe RBMs for tubes with diameter <12 nm.

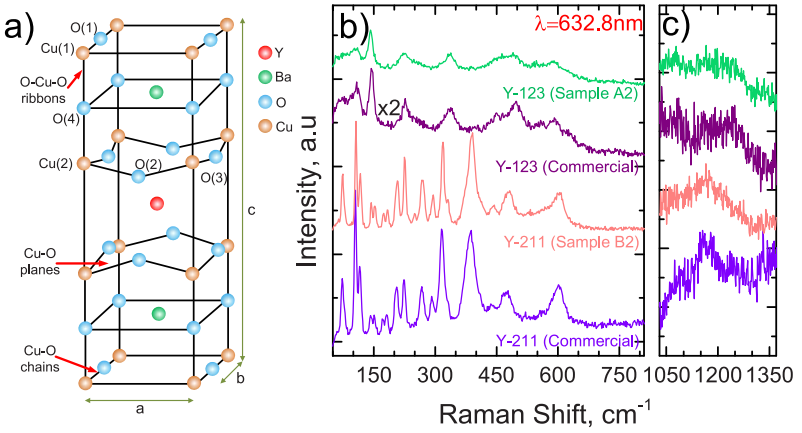

Figure 4. (a) Orthorhombic unit cell of Y-123 (b,c) Raman spectra of samples A2 and B2 compared to commercial Y-123 and Y-211 powders measured at 632.8 nm.

Figure 2b shows that the tail of a broad RBM band is observed at ~30−50 cm^{-1}. This gives a diameter distribution ~7−10 nm, matching that of the inner walls of our MWNTs.[31]

Figures 2a,b indicate that the precursor nitrate salt mixtures Y123P and Y211P (prepared as described in Methods) have Raman bands in the low frequency region. These are usually assigned to vibrations of water molecules[45] and nitrate ions.[45,46] We also observe a peak at ~1045 cm^{-1}, Figure 2c, labeled ν_1. We assign this to the symmetric, in-phase N−O stretching from NO_3^- in $Ba(NO_3)_2$ and hydrated $Y(NO_3)_3$ precursor salts.[47−49] The low frequency component at ~1034 cm^{-1} in Y211P is due to the higher cation molar fraction of hydrated $Y(NO_3)_3$ in the precursors.

The Raman spectra of samples A and B, which contain Y-123, Y-211 precursor salts in the same cation molar ratio as Y123P, Y211P, in addition to MWNTs, show a strong carbon signal, Figure 2a. The overall shape of the carbon-related Raman spectra is similar to that of the original MWNT powder. The low frequency bands in the mixtures are a signature of the precursor salts, and overshadow any RBM. We also observe the ν_1 peak ~1045 cm^{-1} from the hydrated nitrate salts.

We then consider the Raman spectra of samples A2 (Y-123) and B2 (Y-211) and their commercial counterparts, Figure 3. We do not detect any D or G peaks. We thus conclude that the MWNTs have been completely decomposed during the repeated high-temperature calcination in air. Sample A2 shows peaks in the. ~350−600 cm^{-1} region, see Figure 4b. In general, for YBCO, the modes above ~300 cm^{-1} are related to oxygen.[50] The unit cell of Y-123 (Figure 4a) consists of basal Cu planes partially filled with O atoms and separated from the CuO_2 planes (Cu2−O2,O3) by BaO (Ba−O4) planes, see ref 51. The Raman peaks at ~335−440 cm^{-1} are usually assigned to out-of- and in-phase vibrations of these O2−O3 oxygen atoms with the CuO_2 planes.[52,53] The peak ~490−500 cm^{-1} is assigned to the vibration of oxygen O4 in apical

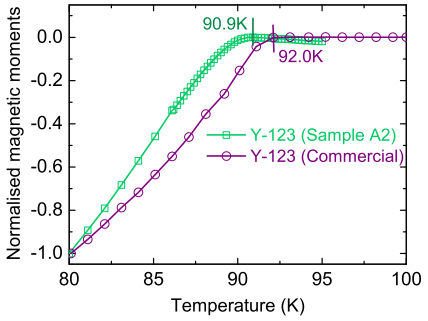

Figure 5. Comparison of T_c of commercial Y-123 powder with that of Y-123 powder (sample A2) fabricated from the CNT templates.

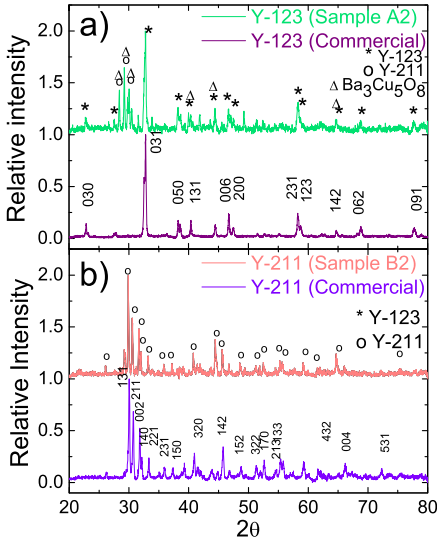

Figure 6. XRD patterns of (a) sample A2 (Y-123) and (b) sample B2 (Y-211), compared with commercial powders.

sites of the orthorhombic phase of Y-123.[52−54] Sample A2 therefore exhibits peaks characteristic of Y-123,[53,55,56] as seen from the comparison with the commercial Y-123 powder in Figure 4b. The bands ~585−640 cm^{-1} are assigned to oxygen atom vibrations in the O−Cu−O ribbons (see Figure 4a).[57]

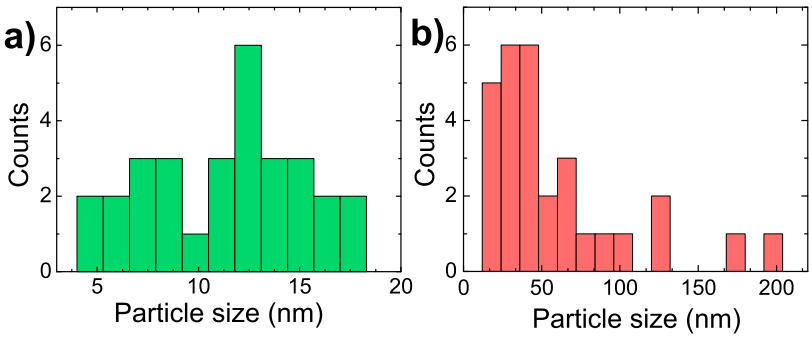

Figure 7. Particle size distribution for (a) sample A2 (Y-123) and (b) sample B2 (Y-211).

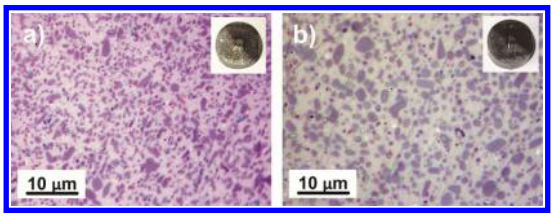

Figure 8. Microstructure comparison of YBCO single grain samples fabricated using (a) Y-211 (sample B2), and (b) commercial Y-211. Insets: Photographs of the respective specimens (16 mm diameter).

The B2 spectrum is also comparable to commercial Y-211.[50,58] For a detailed assignment see ref 50. The peaks ~317, 390, and 477 cm^{-1} are due to vibration of O2, O3 oxygen atoms,[50] and that ~600 cm^{-1} is due to vibration modes of O3 oxygen atoms in Y-211.[50,58] The band ~1169 cm^{-1} in Figure 4c was assigned to low energy electronic excitations of Cu(II) in Y-211.[58,59]

To further study the purity of the superconducting phase, we measure T_c of sample A2 and compare it to Y-123, Figure 5 (see Methods for measurements details). A2 shows superconducting behavior with an onset $T_c = 90.9$ K, comparable to the Y-123 powder. This indicates that the use of CNTs as templates to fabricate nanostructured Y-123 does not affect T_c.

The lattice structure of the Y-123 and Y-211 nanopowders (A2 and B2) is determined using a D500/501 X-ray diffractometer, Figure 6a,b. XRD patterns of commercial powders are also measured. The A2,B2 XRD peaks coincide with those of commercial powders. This demonstrates that the CNT template does not affect the lattice structure of the final powder. XRD further confirms that the mixture of the nitrates of Y, Ba, and Cu decomposes to form stoichiometric Y-123 and Y-211 in the presence of CNTs. We observe a small amount of Y-211 in the A2 XRD pattern. Note that, to balance the overall chemical composition, an appropriate amount of $Ba_3Cu_5O_8$ should be present in this sample. As the main peaks of $Ba_3Cu_5O_8$ overlap those of Y-123 and Y-211, it is not easy to identify the exact quantity. However, a trace of Y-211 and $Ba_3Cu_5O_8$ in the final powder is not significant with regards to the development of YBCO superconductors, since the two phases are mixed and react peritectically to form Y-123 during melt-processing.[4] The amount of Y-211 and $Ba_3Cu_5O_8$ can be reduced by calcining A2 repeatedly at 880 °C, or slightly higher (*e.g.*, ~900 °C).

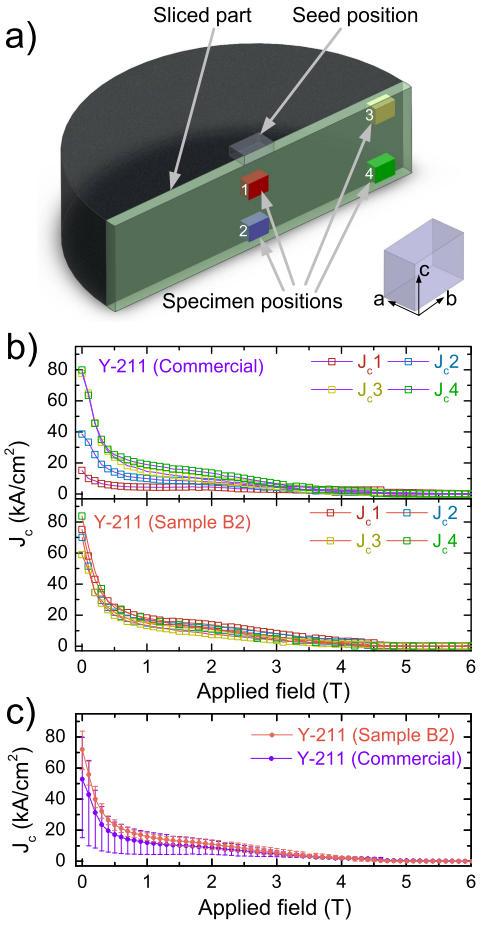

Figure 9. (a) Schematic of the specimens cut from the single grain sample, in order to study the spatial variation of the superconducting properties. ~1 mm slice (light green) is taken from the middle of the grain, and then specimens are cut from this in four selected locations relative to the seed position. (b) Measured J_c of the samples fabricated using Y-211 (sample B2) and commercial Y-211 for the four different specimens, as indicated in panel a. (c) Comparison of average J_c. The bars indicate the maximum and minimum measured values. The J_c values at different applied fields are derived from Equation (2) in Methods.

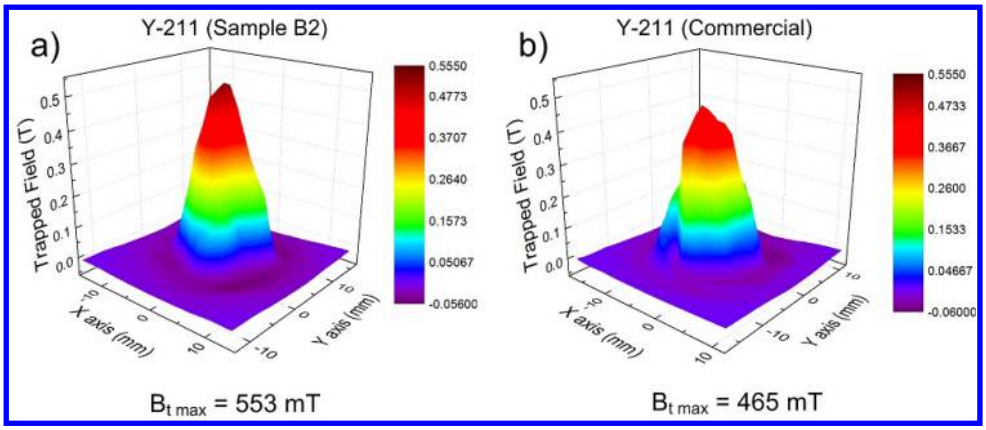

Figure 10. Comparison of the trapped field of the single grain fabricated from Y-211 (sample B2) and commercial Y-211.

To determine their dimensions and distributions, the ground, calcined powders (A2, B2) are next examined by transmission electron microscopy (TEM). Drops of A2 and B2 prepared by mixing the powders with water are dispensed on holey carbon grids. We use a Tecnai T20 high resolution TEM with an acceleration voltage of 200 kV in energy filtered mode. The particles have different morphologies and sizes, ranging from 4 to 100 nm, with some agglomerates as large as 500 nm, especially in B2. The statistical analysis is based on inspection of over 40 TEM images. Figure 7a shows the particle size distribution for Y-123 (A2) and Y-211 (B2). We find that A2, on average, consists of 12 nm particles, whereas 30% of the particles in B2 are >75 nm. The remainder 70% particles in B2 have an average size of ~30 nm.

The particle size in B2 is also examined in the melt-processed single grain sample, Figure 8a, fabricated using B2 with commercial Y-123 as matrix. Figure 8b compares the microstructure of this sample with a YBCO single grain containing commercial Y-211 and Y-123. Normally, superconducting YBCO single grains contain a Y-123 phase matrix with Y-211 particles as inclusions.[4,11,12,60] The Y-211 particle size during melt-processing typically increases to between 1 and 5 μm at high temperature (*i.e.*, 1000 °C for >100 h).[61] The comparison between Figure 8a and 8b confirms that the particle size of sample B2 remains less than 1 μm. This is due to the nanometer dimensions of the starting B2 powder.

For type II HTS, J_c can be determined from[62]

$$J_c = \frac{N\mu_o H_c^2 \pi \xi d}{2B} \quad (1)$$

where μ_o is the permeability of free space, N is the number of pinning centers in a unit volume, H_c is the critical magnetic field, ξ is the coherence length, d is the size of the nonsuperconducting inclusion (*i.e.*, pinning center) and B is the magnetic field. Increasing the number of pinning centers in a given volume is necessary to increase J_c.[11,15] We observe smaller particles of Y-211 in Figure 8a compared to Figure 8b. Thus, there will be more pinning centers in the YBCO single grain prepared from sample B2 compared to commercial Y-211. Therefore we expect the former sample to exhibit higher J_c and trapped field.

In general, for single grain samples fabricated *via* TSMG, J_c varies across the sample.[63,64] For example, J_c is usually the lowest under the seed,[63,64] and gradually increases away from it.[64] The schematic in Figure 9a shows the four specimen positions that we used to measure J_c relative to the seed, cut from the slice (shown in light green) taken from the single grain. The axes relative to the sample orientation are also shown. The color-coded plot in Figure 9b compares J_c of the four colored specimens measured in single grain samples fabricated from commercial Y-211 and zY-211(B2). The J_c values in Y-211(B2) are very uniform compared to commercial Y-211. This indicates a uniform distribution of pinning centers. Figure 9c plots the average J_c from the same four pieces as Figure 9a,b. The highest and lowest J_c at each point are also shown. We observe a ~20% improvement in average J_c at zero field compared to the sample prepared from commercial Y-211. This improvement is of significant importance for a range of applications,[2] as higher J_c supports superconductivity with stronger fields.

Bulk HTS can potentially sustain considerably higher magnetic (trapped) fields than conventional permanent magnets.[2,4,65] The trapped field is proportional to J_c and the volume of the superconductor.[2,12,66] It is more difficult to achieve a higher trapped field compared to higher J_c because of the presence of large voids and cracks in the bulk sample[2] which block the supercurrent. As shown in Figure 10a, we record 553 mT trapped field for the single grain 16 mm sample. This is ~20% higher than the sample containing commercial Y-211 (see Figure 10b) and is comparable to that usually obtained from similar samples with 20–25 mm diameter[67] for the same experimental conditions. However, smaller samples are easier to

fabricate due to the lower furnace requirements and shorter time of melt-processing. Also, from the application point of view, the bulk superconductor fabricated using sample B2, with its higher trapped field can replace larger samples, *e.g.*, in superconducting bearings,[2] reducing the overall cost and size of implementations.

CONCLUSIONS

We demonstrated a fabrication process to produce nanosized nonsuperconducting Y-211 and superconducting Y-123 powders using CNTs as templates. The resulting average particle size is ~12 and ~30 nm, respectively. The use of CNTs does not affect either the superconducting transition temperature, or the lattice structure. We recorded a trapped field 553 mT for a 16 mm diameter sample containing nano size Y-211 and commercial Y-123, with ~20% improvement in average J_c at zero field compared to a sample containing commercial Y-211 and Y-123. Our nano-templating method is general and can be used to fabricate other nanosize powders, such as Y-2411(M).[8,10]

METHODS

Preparation of Nitrate Solutions of Y-123 and Y-211. $Y(NO_3)_3$ (Alfa, 99.9% purity), $Ba(NO_3)_2$ (Alfa, 99.9%), and $Cu(NO_3)_2$ (Alfa, 99.9%) precursor powders are weighed in the appropriate cation molar ratios to form the $YBa_2Cu_3O_{6.5}$ and Y_2BaCuO_5 phases, respectively, according to the following empirical relations. Note that the final oxygen content in the nonstoichiometric samples may vary according to the fabrication method.

$$Y(NO_3)_3 + 2Ba(NO_3)_2 + 3Cu(NO_3)_2 \rightarrow YBa_2Cu_3O_{6.5}$$

$$2Y(NO_3)_3 + Ba(NO_3)_2 + Cu(NO_3)_2 \rightarrow Y_2BaCuO_5$$

The nitrate powders are dissolved in distilled water at room temperature to yield a ~0.6 mol/L concentration of Y-123 and Y-211. As a reference, an aliquot of the Y-123 and Y-211 solutions is dried without the MWNTs: samples Y123P and Y211P, respectively.

Dispersion of CNTs. We use MWNTs with ~10−20 nm outer diameter and ~5−10 nm inner diameter (Sigma-Aldrich, 636525).[31] 8 mg MWNTs are dispersed in 20 mL of deionized (DI) water by ultrasonication for 40 min (Branson, 450A, 20−25 °C). The resulting dispersions are then centrifuged using a MLA-130 fixed-angle rotor (Beckman) for 2 h at a *g*-force of 1500−2000*g* (where *g* denotes the acceleration due to gravity). The supernatants, free from large MWNT bundles and other carbonaceous impurities, are then decanted from the centrifuge tube.

Fabrication of Superconducting Powders Using CNTs as Templates. The CNT dispersion is mixed with the $YBa_2Cu_3O_{6.5}$ and Y_2BaCuO_5-based nitrate solution (1:4 vol %) using tip ultrasonication (Hielscher) for 10 min at 40 W output power. This is then dried in air for 4 days, then calcined in an Ar atmosphere at 600 °C for 10 h to eliminate the nitrates. Finally, the powders are calcined repeatedly (three times) at 880 °C for 10 h in air to eliminate carbon and form the target Y-123 and Y-211 phases.

Fabrication of Superconducting Single Grain Using Nanostructured Y-211 (B2). Superconducting YBCO single grains are fabricated *via* TSMG.[12] Powders of Y-123 (99.9% purity), Y-211 (sample B2), and Pt (to inhibit coarsening of the Y-211 particles during melt-processing at high temperature[7]) are mixed in a composition of (70 wt % Y-123 + 30 wt % Y-211) + 0.1 wt % Pt. 10 g are then pressed uniaxially into a pellet of diameter 20 mm. A NdBCO seed is placed on the top surface of the pellet at room temperature to promote heterogeneous nucleation during melt processing. The sample is then heated to 1045 °C for 1.0 h, cooled to 1015 °C at a rate of 120 °C/h, then slow cooled to 975 at 0.4 °C/h, and furnace cooled to room temperature. As a result, the diameter shrinks to 16 mm. The sample is finally polished using a diamond spray, and its microstructure is analyzed using a Nikon ECLIPSE ME600 optical microscope. Finally, the particle size of Y-211 inside the bulk sample is compared with that of a standard sample fabricated using commercially available Y-211.

Measurements of T_c, J_c, and Trapped Field. The sample is first cooled to a temperature lower than T_c (*i.e.* zero-field cooled condition). Then T_c is measured with an applied field of 10 Oe, using a superconducting quantum interface device (SQUID). For the trapped field measurements, the top surfaces of the samples are polished flat. The trapped magnetic field profiles at the samples' top surfaces are measured using a homemade Hall probe flux-scanning system. Samples are then field cooled, followed by the application of 0.8 T. The Hall probes (20 probes in a line) of the system are positioned 0.5 mm above the sample surface and rotated 360 degrees during the measurements. Then the single grain samples are sliced from the middle as for Figure 9(a). The slices are further cut into smaller pieces for J_c measurements. The size of the specimens are ~1.5 × 1.5 × 1.0 mm^3. From the magnetic moments obtained from a SQUID, an extended Bean model is employed to calculate J_c (A/cm^2) at 77 K using the relation[68]

$$J_c = \frac{20\Delta m}{a\left(1 - \frac{a}{3b}\right)abc} \quad (2)$$

where Δm (emu) represents the difference in magnetic moment observed in the M−H loops for increasing and decreasing field cycles with the applied field perpendicular to the *ab* plane and *a*, *b*, and *c* are the dimensions (cm) of the sample with $a < b$.

Conflict of Interest: The authors declare no competing financial interest.

Acknowledgment. Y.S. acknowledges funding from EPSRC (EP/H049657/1), TH from King's College, Cambridge, and the Royal Academy of Engineering, ACF from the ERC Grant NANOPOTS and a Royal Society Wolfson Research Merit Award.

REFERENCES AND NOTES

1. Shiohara, Y.; Endo, A. Crystal Growth of Bulk High-T_c Superconducting Oxide Materials. *Mater. Sci. Eng., R.* **1997**, *19*, 1–86.
2. Krabbes, G.; Fuchs, G.; Canders, W. R.; May, H.; Palka, R. *High Temperature Superconductor Bulk Materials*; Wiley-VCH Verlag GmbH & Co.; KGaA, Weinheim, Germany, 2006.
3. Campbell, A. M. Factors Limiting Current Densities in Oxide Superconductors. *Phys. B* **1996**, *216*, 266–268.
4. Murakami, M. *Melt-Processed High-Temperature Superconductors*; World Scientific: Singapore, 1992.
5. Umezawa, A.; Crabtree, G. W.; Liu, J. Z.; Weber, H. W.; Kwok, W. K.; Nunez, L. H.; Moran, T. J.; Sowers, C. H.; Claus, H. Enhanced Critical Magnetization Currents Due to Fast Neutron Irradiation in Single-Crystal $YBa_2Cu_3O_{7-x}$. *Phys. Rev. B* **1987**, *36*, 7151–7154.
6. Iida, K.; Nadendla, H. Babu; Reddy, E. S.; Shi, Y.; Cardwell, D. A. The Effect of Nanosize ZrO_2 Powder Addition on the Microstructure and Superconducting Properties of Single-Domain Y-Ba-Cu-O Bulk Superconductors. *Supercond. Sci. Technol.* **2005**, *18*, 249–254.
7. Izumi, T.; Nakamura, Y.; Shiohara, Y. Doping Effects on Coarsening of Y_2BaCuO_5 Phase in Liquid. *J. Mater. Res.* **1993**, *8*, 1240–1246.
8. Babu, N. H.; Reddy, E. S.; Cardwell, D. A.; Campbell, A. M.; Tarrant, C. D.; Schneider, K. R. Artificial Flux Pinning Centers

in Large, Single-Grain (RE)-Ba-Cu-O Superconductors. *Appl. Phys. Lett.* **2003**, *83*, 4806–4808.
9. Kumar, P.; Pillai, V.; Bates, S. R.; Shah, D. O. Preparation of $YBa_2Cu_3O_{7-x}$ Superconductor by Coprecipitation of Nanosize Oxalate Precursor Powder in Microemulsions. *Mater. Lett.* **1993**, *16*, 68–74.
10. Pathak, S. K.; Yeoh, W. K.; Babu, N. H.; Shi, Y.; Iida, K.; Strasik, M.; Cardwell, D. A. Fabrication of High Performance Y-123/Y-24Nb1/Ag Single Grain Composites. *Phys. C* **2009**, *469*, 1173–1177.
11. Lo, W.; Cardwell, D. A.; Dewhurst, C. D.; Dung, S. L. Fabrication of Large Grain YBCO by Seeded Peritectic Solidification. *J. Mater. Res.* **1996**, *11*, 786–794.
12. Cardwell, D. A. Processing and properties of large grain (RE)BCO. *Mater. Sci. Eng., B* **1998**, *53*, 1–10.
13. Griffith, M. L.; Huffman, R. T.; Halloran, J. W. Formation and Coarsening Behavior of Y_2BaCuO_5 from Peritectic Decomposition of $YBa_2Cu_3O_{7-X}$. *J. Mat. Res.* **1994**, *9*, 1633–1643.
14. Sawano, K.; Morita, M.; Tanaka, M.; Sasaki, T.; Kimura, K.; Takebayashi, S.; Kimura, M.; Miyamoto, K. High Magnetic Flux Trapping by Melt-Grown YBaCuO Superconductors. *Jpn J. Appl. Phys.* **1991**, *30*, L1157.
15. Murakami, M. Processing of Bulk YBaCuO. *Supercond. Sci. Technol.* **1992**, *5*, 185.
16. Website URL: http://www.material-sys.com/en/product/, accessed on May 31, 2011.
17. Zhou, L.; Chen, S. K.; Wang, K. G.; Wu, X. Z.; Zhang, P. X.; Feng, Y. Synthesis of Ultrafine Y_2BaCuO_5 Powder and its Incorporation into YBCO Bulk by Powder Melting Process. *Phys. C* **2001**, *363*, 99–106.
18. Bhargava, A.; Alarco, J.; Mackinnon, I. D. R.; Yamashita, T. Manufacture of Fine Grained Y_2BaCuO_5 Powder by Co-precipitation. *Mater. Lett.* **1995**, *24*, 181–188.
19. Lo, W.; Cardwell, D. A.; Shi, Y. H. Spray Dried Pt-Doped Nd-Ba-Cu-O Precursor Powder for Seeded Peritectic Processing of Large Superconducting Grains. *Mater. Sci. Eng., B.* **1999**, *65*, 1–10.
20. Li, F.; Vipulanandan, C.; Zhou, Y. X.; Salama, K. Nanoscale Y_2BaCuO_5 Particles for Producing Melt-Textured YBCO Large Grains. *Supercond. Sci. Technol.* **2006**, *19*, 589–595.
21. Kumar, N. D.; Rajasekharan, T.; Muraleedharan, K.; Banerjee, A.; Seshubai, V. Unprecedented Current Density to High Fields in $YBa_2Cu_3O_{7-d}$ Superconductor through Nano-Defects Generated by Preform Optimization in Infiltration Growth Process. *Supercond. Sci. Technol.* **2010**, *23*, 105020.
22. Li, F.; Vipulanandan, C. Characterization of Y_2BaCuO_5 Nanoparticles Synthesized by Nano-emulsion Method. *J. Nanopart. Res.* **2007**, *9*, 841–852.
23. Nariki, S.; Matsui, M.; Sakai, N.; Murakami, M. Refinement of RE211 Particles in Melt-Textured RE-Ba-Cu-O Bulk Superconductors. *Supercond. Sci. Technol.* **2002**, *15*, 679–682.
24. Chikkannanavar, S. B.; Smith, B. W.; Luzzi, D. E. In *Carbon Nanotubes: Properties and Applications*; O'Connell, M. J., Ed.; CRC Press: Boca Raton, FL, 2006.
25. Ajayan, P. M.; Stephan, O.; Redlich, P.; Colliex, C. Carbon Nanotubes as Removable Templates for Oxide Nanocomposites and Nanostructures. *Nature* **1995**, *375*, 564–567.
26. Sun, Z.; Zhang, H.; Zhao, Y.; Huang, C.; Tao, R.; Liu, Z.; Wu, Z. Thermal-Stable Carbon Nanotube-Supported Metal Nanocatalysts by Mesoporous Silica Coating. *Langmuir* **2011**, *27*, 6244–6251.
27. Whitby, R. L. D.; Hsu, W. K.; Boothroyd, C. B.; Brigatti, K. S.; Kroto, H. W.; Walton, D. R. M. WS_2 Layer Formation on Multiwalled Carbon Nanotubes. *Appl. Phys. A: Mater. Sci. Process.* **2003**, *76*, 527–532.
28. Shi, Y.; Babu, H. N.; Iida, K.; Cardwell, D. A. Mg-doped Nd-Ba-Cu-O Generic Seed Crystals for the Top-Seeded Melt Growth of Large-Grain (rare earth)-Ba-Cu-O Bulk Superconductors. *J. Mat. Res.* **2006**, *21*, 1355–1362.
29. Hasan, T.; Scardaci, V.; Tan, P. H.; Rozhin, A. G.; Milne, W. I.; Ferrari, A. C. Stabilization and De-bundling of Single-Wall Carbon Nanotube Dispersions in *N*-Methyl-2-Pyrrolidone (NMP) by Polyvinylpyrrolidone (PVP). *J. Phys. Chem. C* **2007**, *111*, 12594–12602.
30. Hasan, T.; Sun, Z.; Wang, F.; Bonaccorso, F.; Tan, P. H.; Rozhin, A. G.; Ferrari, A. C. Nanotube-Polymer Composites for Ultrafast Photonics. *Adv. Mater.* **2009**, *21*, 3874–3899.
31. Website URL: http://www.sigmaaldrich.com/catalog/ProductDetail.do?D7=0&N5=SEARCH_CONCAT_PNO|BRAND_KEY&N4=636525|ALDRICH&N25=0&QS=ON&F=SPEC, accessed on October 21, 2011.
32. Sofie, S. W.; Dogan, F. Effect of Carbon on the Microstructure and Superconducting Properties of $YBa_2Cu_3O_{7-x}$ Melt-Textured Crystals. *Supercond. Sci. Technol.* **2002**, *15*, 735–740.
33. Ferrari, A. C.; Robertson, J. Resonant Raman Spectroscopy of Disordered, Amorphous, and Diamondlike Carbon. *Phys. Rev. B* **2001**, *64*, 075414.
34. Ferrari, A. C.; Robertson, J. Interpretation of Raman Spectra of Disordered and Amorphous Carbon. *Phys. Rev. B* **2000**, *61*, 14095–14107.
35. Piscanec, S.; Lazzeri, M.; Robertson, J.; Ferrari, A. C.; Mauri, F. Optical Phonons in Carbon Nanotubes: Kohn Anomalies, Peierls Distortions, and Dynamic Effects. *Phys. Rev. B* **2007**, *75*, 035427.
36. Ferrari, A. C. Raman Spectroscopy of Graphene and Graphite: Disorder, Electron-Phonon Coupling, Doping and Non-adiabatic Effects. *Solid State Commun.* **2007**, *143*, 47–57.
37. Cancado, L. G.; Jorio, A.; Ferreira, E. H. M.; Stavale, F.; Achete, C. A.; Capaz, R. B.; Moutinho, M. V. O.; Lombardo, A.; Kulmala, T. S.; Ferrari, A. C. Quantifying Defects in Graphene *via* Raman Spectroscopy at Different Excitation Energies. *Nano Lett.* **2011**, *11*, 3190–3196.
38. Chhowalla, M.; Teo, K.; Ducati, C.; Rupesinghe, N.; Amaratunga, G.; Ferrari, A. C.; Roy, D.; Robertson, J.; Milne, W. Growth Process Conditions of Vertically Aligned Carbon Nanotubes Using Plasma Enhanced Chemical Vapor Deposition. *J. Appl. Phys.* **2001**, *90*, 5307–5317.
39. Tan, P.; Zhang, S. L.; Yue, K. T.; Huang, F.; Shi, Z.; Zhou, X.; Gu, Z. Comparative Raman Study of Carbon Nanotubes Prepared by D.C. Arc Discharge and Catalytic Methods. *J. Raman Spectrosc.* **1997**, *28*, 369–372.
40. Telg, H.; Maultzsch, J.; Reich, S.; Hennrich, F.; Thomsen, C. Chirality Distribution and Transition Energies of Carbon Nanotubes. *Phys. Rev. Lett.* **2004**, *93*, 177401.
41. Rao, A. M.; Richter, E.; Bandow, S.; Chase, B.; Eklund, P. C.; Williams, K. A.; Fang, S.; Subbaswamy, K. R.; Menon, M.; Thess, A.; *et al.* Diameter-Selective Raman Scattering from Vibrational Modes in Carbon Nanotubes. *Science* **1997**, *275*, 187–191.
42. Meyer, J. C.; Paillet, M.; Michel, T.; Moreac, A.; Neumann, A.; Duesberg, G. S.; Roth, S.; Sauvajol, J. L. Raman Modes of Index-Identified Freestanding Single-Walled Carbon Nanotubes. *Phys. Rev. Lett.* **2005**, *95*, 217401.
43. Jorio, A.; Saito, R.; Hafner, J. H.; Lieber, C. M.; Hunter, M.; McClure, T.; Dresselhaus, G.; Dresselhaus, M. S. Structural (n,m) Determination of Isolated Single-Wall Carbon Nanotubes by Resonant Raman Scattering. *Phys. Rev. Lett.* **2001**, *86*, 1118–1121.
44. Araujo, P. T.; Doorn, S. K.; Kilina, S.; Tretiak, S.; Einarsson, E.; Maruyama, S.; Chacham, H.; Pimenta, M. A.; Jorio, A. Third and Fourth Optical Transitions in Semiconducting Carbon Nanotubes. *Phys. Rev. Lett.* **2007**, *98*, 067401.
45. Kanno, H; Hiraishi, J. Raman Study of Aqueous Rare Earth Nitrate Solutions in Liquid and Glassy States. *J. Phys. Chem.* **1984**, *88*, 2787–2792.
46. Guofa, L.; Tongshun, S.; Yongnian, Z. Infrared and Raman Spectra of Complexes about Rare Earth Nitrate with Schiff Base from O-vanillin and 1-naphthylamine. *J. Mol. Struct.* **1997**, *412*, 75–81.
47. Mathieu, J. P.; Lounsbury, M. The Raman Spectra of Metallic Nitrates and the Structure of Concentrated Solutions of Electrolytes. *Discuss. Faraday Soc.* **1950**, *9*, 196–207.
48. Waterland, M. Symmetry breaking effects in NO_3: Raman Spectra of Nitrate Salts and *ab initio* Resonance Raman Spectra of Nitrate−Water Complexes. *J. Chem. Phys.* **2001**, *114*, 6249.
49. Waterland, M. Far-ultraviolet Resonance Raman Spectroscopy of Nitrate Ion in Solution. *J. Chem. Phys.* **2000**, *113*, 6760.

50. Abrashev, M. V.; Iliev, M. N. Polarized Raman Spectra of Y_2BaCuO_5: Normal-Mode Assignment from Substitutions for Y and Ba. *Phys. Rev. B.* **1992**, *45*, 8046.
51. Faulques, E. In *Materials Synthesis and Characteriztion*; Perry, D. L., Ed.; Plenum Press: New York, 2006.
52. Thomsen, C.; Litvinchuk, A. P.; Schonherr, E.; Cardona, M. Chain-oxygen vibrations in $YBa_2Cu_3O_{7-\sigma}$ and $YBa_2Cu_4O_8$. *Phys. Rev. B* **1992**, *45*, 8154–8157.
53. Camerlingo, C.; Delfino, I.; Lepore, M. Micro-Raman Spectroscopy on YBCO Films During Heat Treatment. *Supercond. Sci. Technol.* **2002**, *15*, 1606–1609.
54. Huong, P. V. Microstructure of High Temperature Superconductor Thin Films as Studied by Micro-Raman Spectroscopy. *Phys. C* **1991**, *180*, 128–131.
55. Barboy, I.; Camerlingo, C.; Bar, I.; Bareli, G.; Jung, G. Micro-Raman Spectroscopy of Laser Processed $YBa_2Cu_3O_{7-d}$ Thin Films. *J. Appl. Phys.* **2011**, *110*, 033912.
56. Palles, D.; Poulakis, N.; Liarokapis, E.; Conder, K.; Kaldis, E.; Muller, K. A. Raman Study of the Oxygen Anharmonicity in $YBa_2Cu_3O_x$ ($6.4 < x < 7.0$) Superconductors. *Phys. Rev. B* **1996**, *54*, 6721–6727.
57. Burns, G.; Dacol, F. H.; Feild, C.; Holtzberg, F. Raman Measurements of $YBa_2Cu_3O_x$ as a Function of Oxygen Content. *Solid State Commun.* **1991**, *77*, 367–371.
58. Flavell, W. R.; Egdell, R. G. Observation of Electronic Raman Scattering in Y_2BaCuO_5. *Solid State Commun.* **1989**, *69*, 631–633.
59. Udagawa, M.; Ogita, N.; Fukumoto, A.; Utsunomiya, Y.; Ohbayashi, K. Raman and Infrared Spectra of a Green Y_2BaCuO_{5-y}. *Jpn. J. Appl. Phys.* **1987**, *26*, L858.
60. Shi, Y. H.; Yoeh, W.; Dennis, A. R.; Hari Babu, N.; Pathak, P.; Xu, Z.; Cardwell, D. A. Growth Rate of YBCO Single Grains Containing Y-2411(M). *J. Phys. Conf. Ser.* **2010**, *234*, 012039.
61. Yeoh, W. K.; Pathak, S. K.; Yunhua, S.; Dennis, A. R.; Cardwell, D. A.; Babu, N. H.; Strasik, M. Improved Flux Pinning in Y-Ba-Cu-O Superconductors Containing Niobium Oxide *IEEE Trans. Appl. Supercond.* **2009**, *19*, 2970–2973.
62. Campbell, A. M.; Evetts, J. E. Flux Vortices and Transport Currents in Type II Superconductors. *Adv. Phys.* **1972**, *21*, 199–428.
63. Shi, Y.; Babu, N. H.; Cardwell, D. A. Properties of GdBCO Bulk Superconductors Melt-Processed in Air Using a Mg-Doped Nd-Ba-Cu-O Generic Seed Crystal. *Supercond. Sci. Technol.* **2007**, *20*, 38–43.
64. Dewhurst, C. D.; Wai, L.; Cardwell, D. A. Distribution of Critical Current Density in Large $YBa_2Cu_3O_{7-\delta}$ Grains Fabricated Using Seeded Peritectic Solidification. *IEEE Trans. Appl. Supercond.* **1997**, *7*, 1925–1928.
65. Cardwell, D. A.; Hari Babu, N. Processing and Properties of Single Grain (RE)-Ba-Cu-O Bulk Superconductors. *Phys. C* **2006**, *445−448*, 1–7.
66. Tomita, M.; Murakami, M. High-Temperature Superconductor Bulk Magnets that can Trap Magnetic Fields of over 17 T at 29 K. *Nature* **2003**, *421*, 517–520.
67. Xu, C.; Hu, A.; Sakai, N.; Izumi, M.; Hirabayashi, I. Effect of $Gd_2Ba_4CuMoO_y$ Addition on the Band Structure and Spatial Variation of Superconducting Properties in $GdBa_2Cu_3O_{7-\delta}$ Single Domains. *Supercond. Sci. Technol.* **2005**, *18*, 1082–1088.
68. Bean, C. P. Magnetization of High-Field Superconductors. *Rev. Mod. Phys.* **1964**, *36*, 31–39.